CORRECTING INFLOW MEASUREMENTS FROM HAWTS USING A LIFTING-SURFACE CODE

J. Whale,* C. J. Fisichella† and M. S. Selig‡
University of Illinois at Urbana-Champaign
Urbana, IL 61801

Abstract

Aerodynamic performance data from a rotating HAWT blade is typically correlated with measurements of a local inflow angle, obtained by flow angle sensors attached to the leading edge of the blade section. In order to provide accurate performance data for 2D blade-element/momentum codes, the 3D field data must be corrected in terms of the section angle of attack. A 3D Lifting-Surface Inflow Correction Method (LSIM) has been developed with the aid of a vortex-panel code in order to calculate the relationship between the local flow angle and the angle of attack. Sets of inflow correction curves were produced for each spanwise station of interest. The method has been tested using hypothetical 3D input data, based on measurements from the Combined Experiment Rotor at the National Renewable Energy Laboratories and wind tunnel tests at Delft University of Technology. The method was shown to successfully produce a converged solution for the inflow correction curves. The results show the importance of using the 3D LSIM correction instead of a 2D correction, particularly at the inboard sections of the blade where the upwash at the sensor is affected by post stall effects and changes in spanwise circulation distribution on the blade.

*Post-doctoral Research Associate, Dept. Aeronautical and Astronautical Engineering.
†Graduate Student, Dept. Mechanical and Industrial Engineering.
‡Associate Professor, Dept. Aeronautical and Astronautical Engineering, Senior Member AIAA.

1. Introduction

The angle of attack α, as commonly used in aerodynamic models for wind turbines, is defined as the angle between the chord of the blade profile and the effective velocity (the resultant of the components of axial, induced and rotational velocities). Measurements of force coefficients made on a rotating blade, however, are typically correlated with measurements of a local inflow angle β obtained by flow angle sensors protruding from the leading edge of the blade (see Figure 1).

It is desirable to reduce the 3D field measurements in terms of the angle of attack α, in order to provide accurate performance data for 2D blade-element momentum (BEM) codes, dynamic stall models and to compare data from other experimental campaigns. The angle of attack is related to the inflow angle by

$$\alpha = \beta - \alpha_u \qquad (1.1)$$

where α_u is the angle due to the upwash induced at the local inflow point by the bound vorticity on the blade.

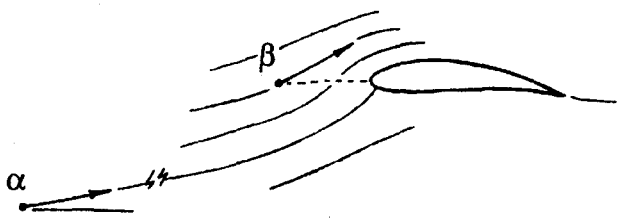

Figure 1. Angle of attack α and local flow angle β for a blade section.

Calculating α_u is a relatively straightforward procedure in a wind tunnel where a 2D airfoil can be positioned at a particular angle α and a

probe used to measure the local inflow angle β at a point. There are significant differences, however, between 2D airfoil flow and 3D flow on a rotating blade. This is most noticeable at inboard sections of the blade where the section is experiencing stall. The Coriolis component of the 3D flow suppresses separation; delaying stall and enhancing lift at the blade section. These effects are referred to as 'stall-delay' or 'post-stall' effects.[1, 2]

Various methods have been proposed for calculating the relationship between α and β (and hence the 3D upwash) on a rotating blade. Madsen[3] describes a method that uses BEM to calculate the power curve for the turbine as a function of angle of attack at a particular spanwise position. The measured inflow angle is then adjusted until good agreement is provided between the calculated and measured power curves. The inverse BEM method[4,5] involves assuming the measured normal and tangential forces are uniform over an annulus containing the blade section. The wake-induced velocities are calculated according to momentum theory, yielding the effective velocity vector and subsequently the angle of attack. Brand[6] estimates the angle of attack using a stagnation point method. The measured pressure distribution on a blade section is used to calculate the stagnation point. The intersection of the chord line and a line normal to the surface at the stagnation point yields a stagnation angle, which is used as an estimate for the angle of attack. The position of the point of intersection can be determined using either a 2D airfoil code or from 2D wind tunnel measurements.

Researchers at the National Renewable Energy Laboratories (NREL) have conducted wind tunnel measurements[7] in order to gauge the β–α relationship. A 2D scale model of the blade section was fitted with a flow sensor upstream of the section and placed in a wind tunnel. The 2D upwash obtained from these tests was used an estimate for the 3D upwash. Additionally, static pressure profiles, obtained from 2D wind tunnel tests on a scale model of the blade section, were compared with measured profiles from the rotating blade to find the angle of attack that gave the best agreement between the profiles. Finally, Bruining[8] has incorporated a Schlichting-Truckenbrodt correction in a simplified wake model in order to calculate a 2D upwash.

The current research aims to improve on these essentially 2D methods by calculating the flow field around a HAWT rotor using a 3D vortex panel method. A lifting-surface code is used to model the vorticity in the wake and along the rotor blades. The 3D upwash induced by the bound vorticity is calculated, yielding the β–α relationship at desired spanwise stations as a set of *inflow correction curves*. This paper shows the initial results of using the code to correct 3D data from Phase III of the Combined Experiment Rotor (CER) tests conducted at NREL.

2. The Inflow Correction Method

An inflow correction method has been developed at the University of Illinois at Urbana-Champaign in order to provide accurate 3D corrections to HAWT aerodynamic data. The method makes use of a lifting-surface code and is referred to as the Lifting-Surface Inflow Correction Method (LSIM). The lifting-surface code was developed by Kocurek[9] and is called Lifting- Surface Aerodynamics and Performance Analysis of Rotors in Axial Flight (LSAF). The code was originally written for the design and analysis of helicopter rotors and then extended to wind turbines.

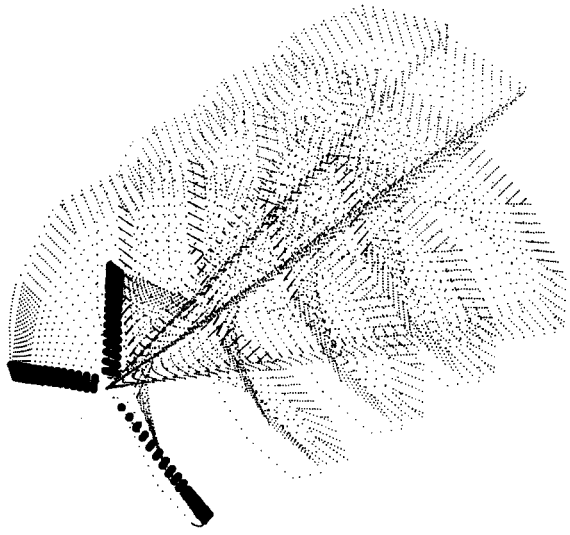

Figure 2. Blade and wake geometry from LSAF.

The code simulates the rotor and the wake as a lattice of lifting surfaces (see Figure 2). A

prescribed wake model is used which allows for roll-up of tip and root vortices. The detailed blade aerodynamics are computed by combining the lifting-surface model with a blade-element analysis that requires as input a table of airfoil performance characteristics. Field velocity routines in the codes allow the computation of the local flow velocity at specified points in the flow.

LSIM evolved from the consideration of the differences in 2D and 3D upwash due to post-stall effects. For inboard stations at post-stall angles of attack, the circulation around a 3D blade section is expected to be greater than that around a 2D section. As Figure 3 illustrates, the 3D post-stall upwash is thus expected to be greater than the 2D upwash.

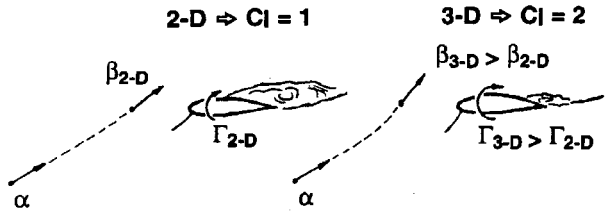

Figure 3. Difference between 2D and 3D flow physics.

Figure 4 shows that for a particular angle of attack past stall, the 3D inflow angle β is higher than the 2D case. This is due to the greater local circulation in the 3D case. Consequently, for a particular inflow angle β past that of 2D stall, the 3D angle of attack α is lower than the angle predicted from the 2D correction curve.

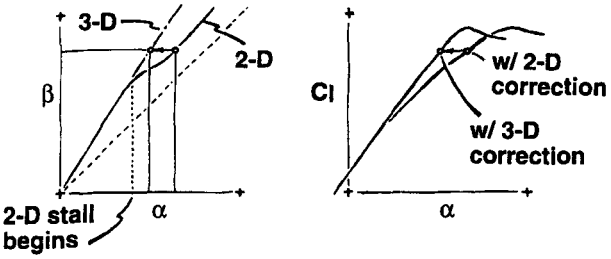

Figure 4. Expected trends for a 3D correction.

Thus, the application of the 3D correction to measured 3D lift data results in a curve that has higher lift at a given α than the curve that has been corrected with 2D data. This higher lift in turn would suggest (through a vortex lattice method) greater values of inflow angle β for that particular α than specified in the β–α curve of Figure 4. It is this interplay between the β–α relationship and the corrected data curves that leads to the concept of an iterative inflow correction method.

The strategy behind LSIM is to initially use an estimate of the 3D β–α relationship and apply this inflow correction to convert the measured raw data into airfoil performance data according to the equations:

$$c_l = c_n \cos\alpha - c_t \sin\alpha \qquad (2.1)$$

$$c_{dp} = c_t \cos\alpha + c_n \sin\alpha \qquad (2.2)$$

The airfoil performance data is then input into the vortex panel code, and the values of α and β are extracted from the output to form a new β–α relationship. The new relationship is used to correct the raw data again and the resulting performance data is input into the code once more. This procedure is repeated until a converged solution for the β–α curve is reached and a final correction can be made to the raw data. Figure 5 outlines this procedure.

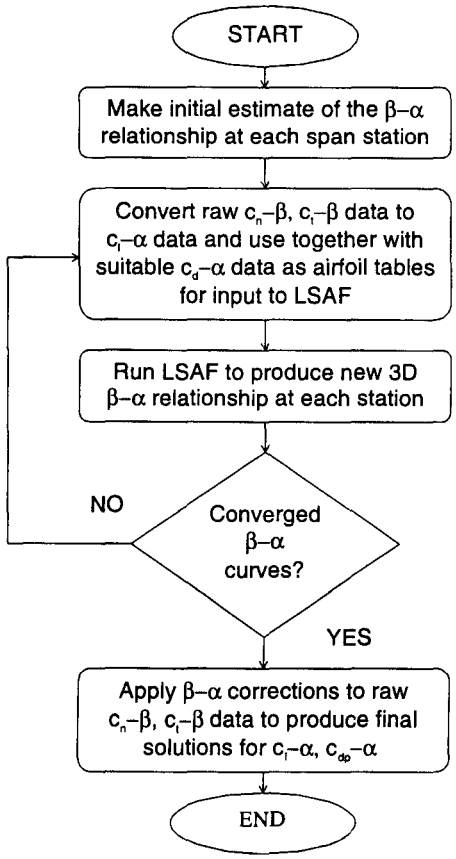

Figure 5. Flowchart outlining the inflow correction method.

3. Available Data

Testing of the correction method requires 3D data from experiments on rotating wind turbine blades. A large amount of 3D data has been gathered from the IEA Annex XIV project (Field Rotor Aerodynamics),[10] which involved the co-ordination of five full-scale aerodynamic test programs. Of these tests, the most comprehensive body of data has been gathered at NREL due to the detailed CER instrumentation. In the latest phase of campaigns on the CER,[11] a highly twisted blade of constant chord without taper was used. With the exception of the root, the blade has an NREL S809 profile (see Figure 6), an airfoil that has been tested in wind tunnels at Delft University of Technology,[12] as well as Ohio State University (OSU) and Colorado State University (CSU).[13]

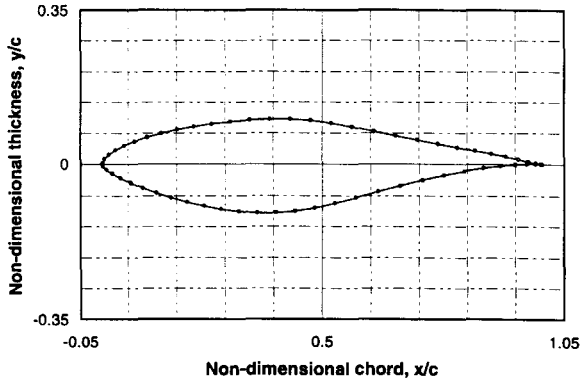

Figure 6. Geometry of the S809 airfoil.

Machine Operation	
Number of blades	3
Rated Power	19.8kW
Power regulation	Stall
Rotor location	Downwind
Cut-in wind speed	6 m/s
Cut-out wind speed	N/A (stall control)
Rotational speed	71.63 rpm
Coning angle	3.42°
Blade Parameters	
Type	NREL in-house
Profile	S809
Chord	0.4572 m
Thickness	0.096 m
Length	5.05 m
Set Angle	Approx. 3°
Root Extension	0.723 m

Table 1. Parameters for the Phase III CER tests.

Table 1 shows the blade geometry and operating parameters for the CER during Phase III of the measurement campaigns. Measurements of the local inflow, at a distance in front of the leading edge of the blade equal to 79% of the chord, were made with lightweight flow sensor flags for spanwise stations of 30%, 47%, 63% and 80% of blade radius.

'Steady' CER data was produced by binning cycle-averaged data where the data cycles were chosen using baseline criteria on the inflow variance and yaw error.[11] Plots of binned normal and tangential blade force coefficients versus local flow angle for the Phase III tests are shown in Figures 7(a) and 7(b).

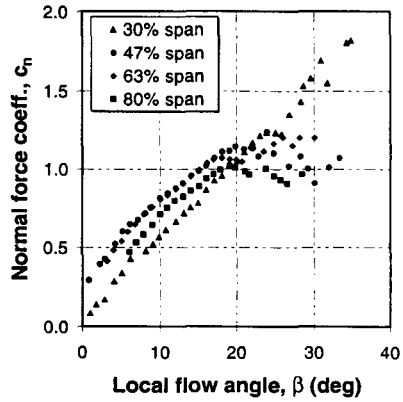

(a) Normal force coefficient versus local flow angle

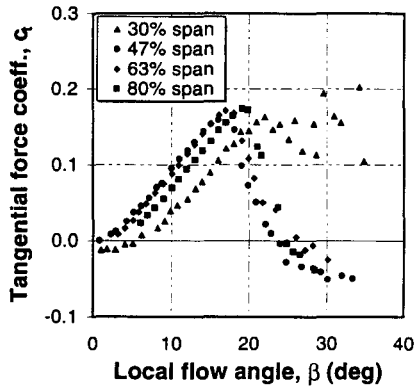

(b) Tangential force coefficient versus local flow angle

Figure 7. Performance data from Phase III of the CER tests.

Examining Figure 7, there are some puzzling features of the CER data that either do not fit with the trends of the graphs or are not expected from the concept of the flow physics outlined in Figure 3. At 30% span, pre-stall

values of c_n appear lower and post-stall values of c_t are higher than the trends with spanwise position observed in the graph. At 63% span the post-stall values of c_n are higher than at 47% span which appears inconsistent with the concept of enhanced lift at inboard stations.

Researchers at NREL are attempting to resolve some of the questions regarding this data by re-calibration of the CER pressure measurement system. For current purposes, it was decided to test LSIM by producing a set of 'hypothetical' performance curves for the CER for each spanwise station.

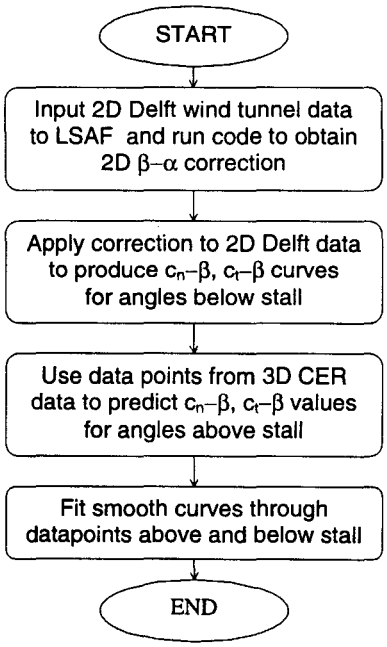

Figure 8. Flowchart for producing hypothetical performance data.

Figure 8 explains the procedure in producing this hypothetical data. The concept involves using 2D performance data for the S809 airfoil from wind tunnel tests at Delft University of Technology[12] for pre-stall behavior of the hypothetical curves and using the 3D CER Phase III data as a guide in estimating the post-stall behavior of the curves. The hypothetical performance curves produced in this manner are shown in Figure 9.

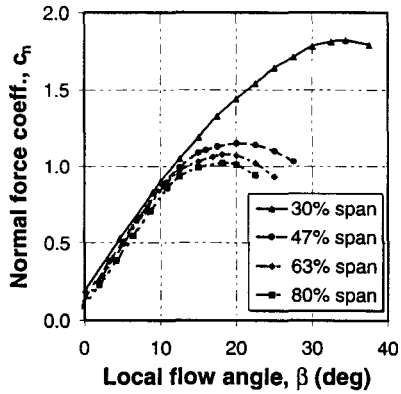

(a) Normal force coefficient versus local flow angle

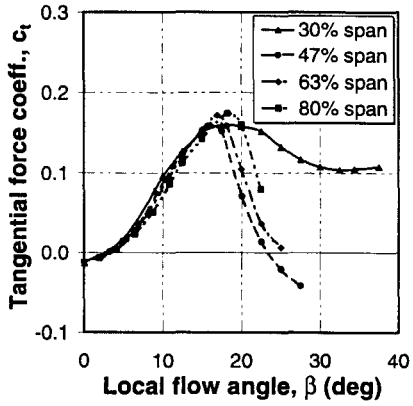

(b) Tangential force coefficient versus local flow angle

Figure 9. Hypothetical performance data based on 2D Delft wind tunnel tests and 3D CER data.

4. Results

The hypothetical data produced in Section 3 was input into the vortex panel code in order to test LSIM. The line of reflection was taken as an initial inflow correction (i.e., $\alpha = \beta$), and lift values were calculated using Eq. (2.1). Drag values for the input tables were taken from 2D Delft data. The inflow correction curves output from the code are shown in Figure 10 for the 30%, 47%, 63% and 80% spanwise stations. This figure, along with the remaining figures of the paper, is placed at the back of the paper to provide a layout for ease of comparison of the plots at the different spanwise stations. The curves of Figure 10 are seen to converge after 4 iterations of the method and are compared with 2D inflow correction curves (i.e., using 2D Delft lift and drag values as input to the code). For each spanwise station, the converged 3D LSIM

curve matches the 2D curve for angles below the stall angle (the stall angle for each station being dependent on the Reynolds number of the flow at that station). Close to the origin of each of the graphs there is a noticeable increase in upwash with increasing spanwise station. This effect is likely to be linked to changes in 3D spanwise circulation.

Looking at the graphs of Figure 10 in more detail, the 30% span curves show a significant departure in the post-stall $\beta-\alpha$ relationship between the 2D and 3D methods. The graph shows $\beta_{3D} > \beta_{2D}$ for some post-stall α, as expected from the theory outlined in Figure 3. In particular, at β = 20 deg there would be difference of around 4 deg between applying a 2D or a 3D correction to the raw measurement data (recall that these differences are based on using 2D and 3D data as input to LSIM as opposed to using a 2D correction curve from a wind tunnel test). At the 47%, 63% and 80% stations, the deviation between the 2D and 3D curves is less significant with a difference of less than 0.5 deg between applying a 2D or a 3D correction across the entire β range.

The converged 3D inflow correction curves are extended over the entire β range of the hypothetical input data and the extended trendlines are used to apply the 3D LSIM corrections to the input data and produce values of lift and pressure drag in accordance with Eqs. (2.1) and (2.2). From the equations it can be seen that applying the inflow correction will affect both the location and values of the 3D performance curves. Convergence of the lift and pressure drag curves with each iteration of LSIM is shown in Figures 11 and 12, respectively, together with the corresponding 2D curves. The errors introduced by extending the inflow correction curves are discussed in Section 5.

At the 30% station in Figure 11, the 3D curve shows higher lift than the 2D curve, as expected from the theory outlined in Figure 3. The graph shows a difference of around 7% in $c_{l\,max}$ between applying a 2D or a 3D correction. The differences between applying the 2D and converged 3D LSIM correction curves are significant, particularly at high angle of attack (e.g. see c_l = 1.5), which is important for peak power prediction. For the 47%, 63% and 80% stations, the difference in c_{lmax} between applying a 2D or 3D correction is less than 0.1% and can be regarded as negligible.

In Figure 12, comparing the 2D curve and the 3D converged solution at 30% span, a 5–10% increase in pressure drag is seen for the 3D correction at post-stall angles. At first glance, this seems contrary to the theory outlined in Figure 3. A closer inspection of the first and second terms of Eq. (2.2), for increasing angle of attack, gives some insight into this phenomenon. Comparing the 3D case to the 2D case, the increase in the component of pressure drag due to the normal force on the blade dominates the decrease in the component of pressure drag due to tangential forces on the blade. The phenomenon of greater 3D drag at inboard stations than 2D drag has also been reported by Björck et al.[14] and warrants further investigation. For the remaining spanwise stations in Figure 12, there appears to be no significant difference between applying a 2D or a 3D correction.

The CER Phase III experimental data of Figure 7 is corrected using the LSIM 'hypothetical' inflow correction curve and contrasted with corrections using OSU/CSU wind tunnel data (the current correction method used by NREL[10]). The comparison of corrected lift and pressure drag data for the 30% span station is shown in Figure 13. In addition, data from the 2D CSU wind tunnel tests[13] at a Reynolds number of 500,000 is plotted.

Comparing the 3D corrected data with the 2D wind tunnel data, the pre-stall values of 3D lift and pressure drag are respectively lower and higher than the wind tunnel data – features which have been queried in Section 3. In the light of these puzzling features of the CER data, it may be wise not to draw too firm conclusions from Figure 13 but to focus on the general trends between the different correction methods employed.

Comparing the 3D corrected data, both graphs show a similar trend, namely that of lower LSIM values for pre-stall angles of attack and higher LSIM values for post-stall angles of attack, which can be attributed to the trend of the respective inflow correction curves. At pre-

stall angles of attack, LSIM predicts lower upwash at 30% than the 2D wind tunnel upwash due to the 3D spanwise circulation distribution. At post-stall angles of attack, LSIM predicts greater upwash at 30% span than the 2D upwash of the wind tunnel method, due to the 3D effects outlined in Figure 3.

5. Discussion of Errors

Application of the correction method shows that the range of calculated α values, corresponding to the range of raw β values, reduces with each iteration. Figure 14 gives an example of the trend in the β–α relationship after 3 iterations of LSIM. The curves are similar to those produced at 30% span using the hypothetical input data. Initially the range of α equals the range of β since our first estimate of the relationship is $\beta=\alpha$. In subsequent iterations, Figure 14 shows that for a set β value, successively smaller values of α are generated.

As Figure 5 illustrates (see Section 2), the β–α relationship is used to correct the raw data which is then input into the vortex panel code. Thus, as shown in Figure 15, the vortex panel code is run with successively smaller ranges of α. The set of β values corresponding to the α values is extracted from the output of the panel code at each iteration, and thus the range of β produced by the code is also reduced. For example, a set of raw data with an initial β range up to 35 deg may produce a β range of only 20 deg once the code has converged. Thus, confidence in the β–α relationship extends only up to 20 deg. In the above work, trendlines were used to extend the β–α relationship over the entire β range, introducing errors in the correction of the raw data at the higher β values. A possible solution to this 'angle–range reduction' problem is to use experimental data with a large β range which, despite undergoing reduction in LSIM, will still produce values for the β–α relationship over the range of interest.

Producing a set of inflow correction curves by running the vortex code over a range of windspeeds 1 m/s – 20 m/s takes approximately 1½ minutes. Automating the iteration scheme will lead to improvements in overall computational time for the method. In addition, LSIM has been tested using the 'steady' data produced by binning cycle-averaged measurements. Further investigations are required to examine the effect of using unsteady 3D field data on the β–α relationship produced by the correction method.

6. Conclusions

A 3D Lifting-Surface Inflow Correction Method (LSIM) has been developed with the aid of a vortex-panel code. The method has been tested using hypothetical 3D input data, based on measurements from the Combined Experiment Rotor (CER) at the National Renewable Energy Laboratories and wind tunnel tests at the Delft University of Technology. The method, tested at each of four spanwise stations (30%, 47%, 63% and 80%), was shown to successfully produce a converged solution for the inflow correction curves (the relationship between the angle of attack and the local flow angle at an upstream probe position).

The method has shown important differences between applying a 3D correction and a 2D correction. This has been illustrated by comparing corrections of CER Phase III data using the new method, and corrections using wind tunnel data. At post-stall angles of attack at 30% span, LSIM predicts higher upwash at the probe than observed in 2D wind tunnel tests. This was an expected result and likely to be due to increased circulation due to 3D lift-enhancement effects on the blade. At pre-stall angles, LSIM predicts less upwash at the probe than measured in 2D wind tunnel tests. This result was less expected but suggests that the 3D spanwise circulation distribution produces less upwash at inboard stations.

At the other stations, further outboard on the blade, the results seem to indicate that there is no significant difference between applying a 2D correction and a 3D correction. This suggests that the flow is essentially 2D at spanwise stations greater than 47% and may indicate that 3D effects do not persist more than halfway along the blade.

In conclusion, LSIM recognizes the important differences between 2D and 3D flows on a wind turbine blade section and appears a very promising method of producing accurate corrections of HAWT measurements. Further

evaluation of the method awaits more field data and the upcoming CER tests in the NASA Ames wind tunnel may provide this opportunity.

Acknowledgments

This work was undertaken with the support of the National Renewable Energy Laboratories under Subcontract No. XCX-7-16466-01 (Technical Monitor: J.L.Tangler). The assistance of M. Hand of NREL in preparing the raw CER data is gratefully acknowledged.

References

[1] Montgomerie, B., "The Influence of 3D Effects in Lift and Drag on the Performance of a Stalled Horizontal Axis Wind Turbine Rotor," Proceedings of the IEA Wind Turbine Aerodynamics Meeting, Denmark, November 1994.

[2] Corrigan, J.J., "Empirical Model for Stall Delay due to Rotation," Proceedings of the American Helicopter Society Aeromechanics Specialists Conference, San Francisco, CA, January 1994.

[3] Madsen, H.A., "Aerodynamics of a Horizontal-Axis Wind Turbine in Natural Conditions," Risø M-2903, Risø National Laboratory, September 1991.

[4] Snel, H., Houwink, R. and Bosschers, J., "Sectional Prediction of Lift Coefficients on Rotating Wind Turbine Blades in Stall," ECN-C-93-052, ECN, May 1993.

[5] Bruining, A., van Bussel, G.J.W., Corten, C.P. and Timmer, W.A., "Pressure Distributions from a Wind Turbine Blade; Field Measurements Compared to 2-dimensional Wind Tunnel Data," DUT-IvW-93065R, Delft University of Technology, August 1993

[6] Brand, A.J., "To Estimate the Angle of Attack of an Airfoil from the Pressure Distribution," ECN-R-94-002, ECN, January 1994.

[7] Shipley, D.E., Miller, M. S., Robinson, M.C., Luttges, M.W. and Simms, D. A. "Techniques for the Determination of Local Dynamic Pressure and Angle of Attack on a Horizontal Axis Wind Turbine," NREL TP-442-7393, May 1995.

[8] Bruining, A., "Aerodynamic Characteristics of a 10m Diameter Rotating Wind Turbine," Delft University of Technology, IW-084R, September 1996.

[9] Kocurek, D., "Lifting Surface Performance Analysis for Horizontal Axis Wind Turbines," SERI/STR-217-3163, June 1987.

[10] Schepers, J.G. (ed.), "Final Report of IEA Annex XIV: Field Rotor Aerodynamics," ECN-C-97-027, June 1997.

[11] Simms, D.A., Robinson, M.S., Hand, M.M. and Fingersh, L.J., "A Comparison of Baseline Aerodynamic Performance of Optimally-Twisted versus Non-Twisted Blades," 15th ASME Wind Energy Symposium, Houston, Texas, February 1996.

[12] Tangler, J. L., Somers, D. M. "NREL Airfoil Families for HAWTs". Proceedings of the Aerodynamics of Wind Turbines 9th Symposium, Stockholm, Sweden, December 1995.

[13] Butterfield, C. P., Musial, W.P. and Simms, D. A. "Combined Experiment Phase I, Final Report," NREL TP – 257-4655, October 1992.

[14] Björck, A., Ronsten, G. and Montgomerie, B., "Aerodynamic Section Characteristics of a Rotating and Non-rotating 2.375m Wind Turbine Blade," FFA TN1995-03, February 1995.

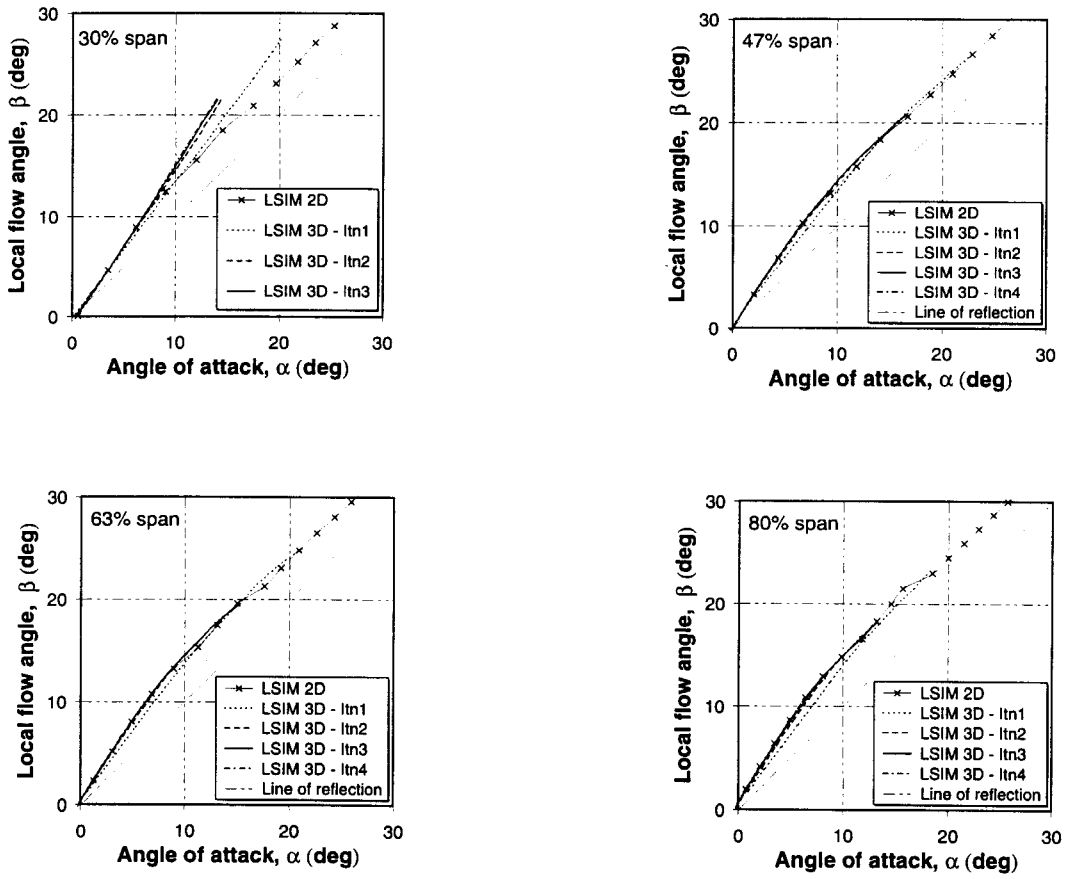

Figure 10. Inflow correction curves produced using hypothetical performance data in LSIM.

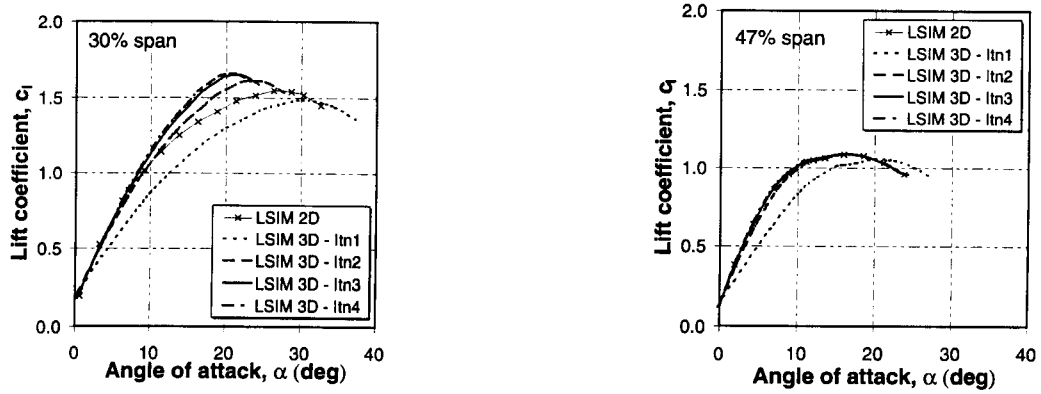

Figure 11. Convergence of hypothetical lift curves using LSIM.

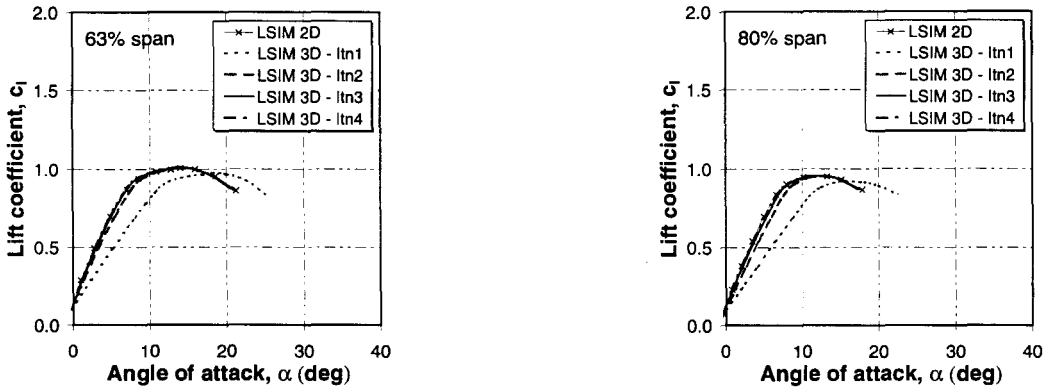

Figure 11(cont.). Convergence of hypothetical lift curves using LSIM.

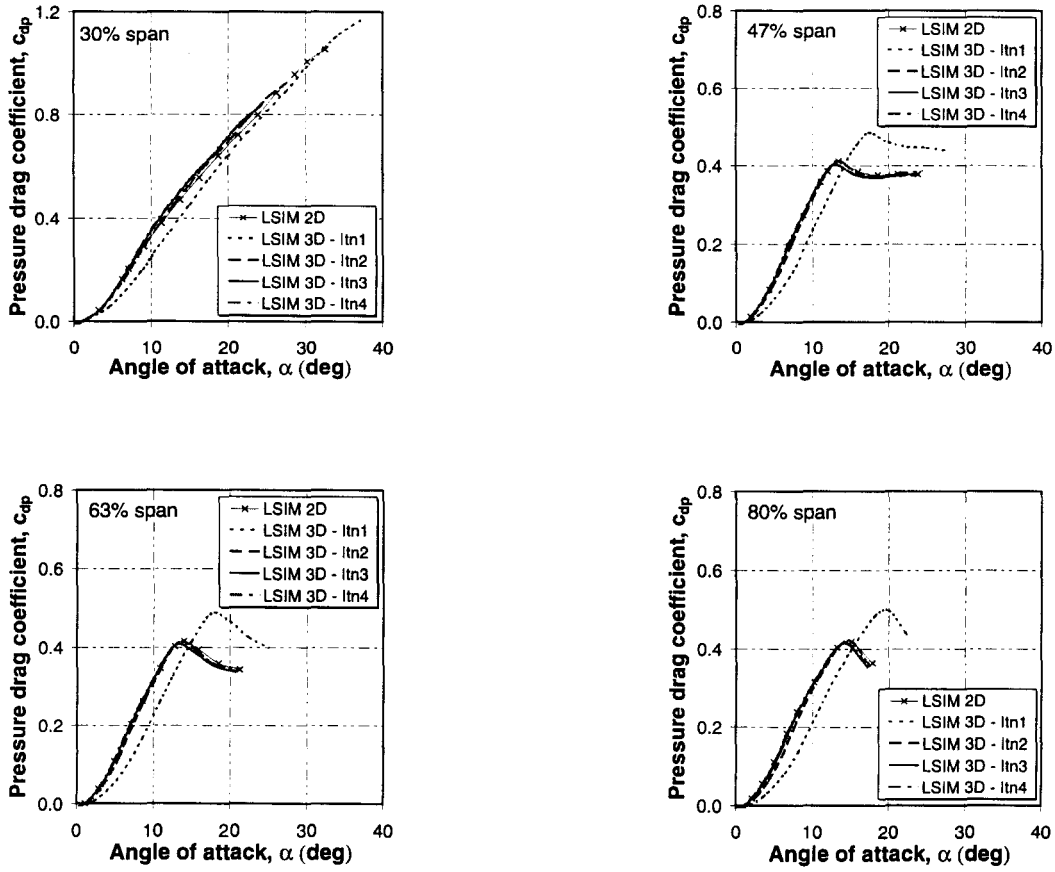

Figure 12. Convergence of hypothetical pressure drag curves using LSIM.

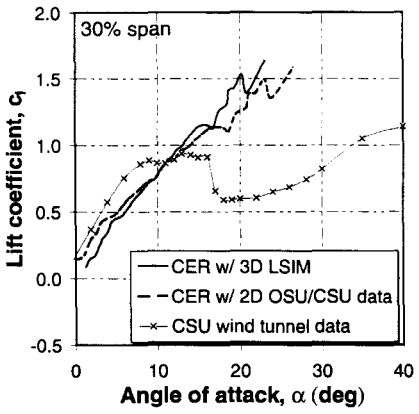

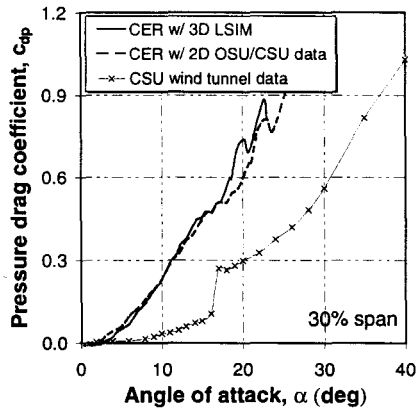

Figure 13. Comparison of corrected CER lift and pressure drag using LSIM and wind tunnel data.

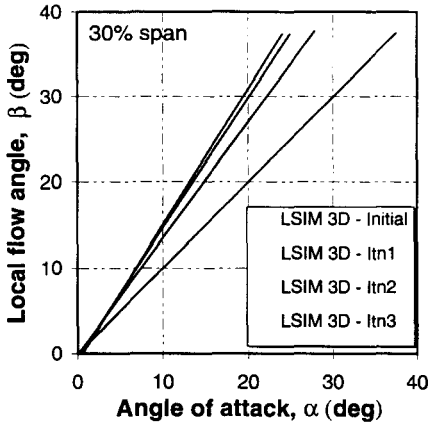

Figure 14. Reduction of the α–range due to the nature of the β–α relationship.

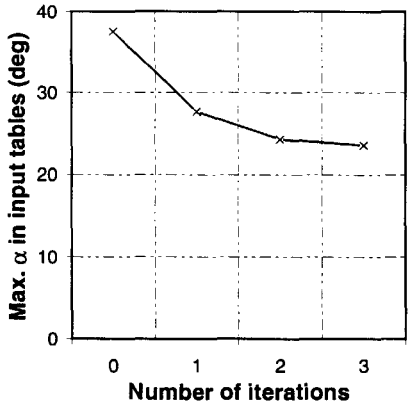

Figure 15. Reduction of the α–range input to the panel code.